2756–2768 Nucleic Acids Research, 2011, Vol. 39, No. 7 Published online 7 December 2010
doi:10.1093/nar/gkq1030

Characterization of *Aquifex aeolicus* ribonuclease III and the reactivity epitopes of its pre-ribosomal RNA substrates

Zhongjie Shi[1], Rhonda H. Nicholson[2], Ritu Jaggi[1] and Allen W. Nicholson[1,2,*]

[1]Department of Chemistry and [2]Department of Biology, Temple University, Philadelphia, PA, USA

Received July 7, 2010; Revised October 6, 2010; Accepted October 10, 2010

ABSTRACT

Ribonuclease III cleaves double-stranded (ds) structures in bacterial RNAs and participates in diverse RNA maturation and decay pathways. Essential insight on the RNase III mechanism of dsRNA cleavage has been provided by crystallographic studies of the enzyme from the hyperthermophilic bacterium, *Aquifex aeolicus*. However, the biochemical properties of *A. aeolicus* (Aa)-RNase III and the reactivity epitopes of its substrates are not known. The catalytic activity of purified recombinant Aa-RNase III exhibits a temperature optimum of ~70–85°C, with either Mg^{2+} or Mn^{2+} supporting efficient catalysis. Small hairpins based on the stem structures associated with the Aquifex 16S and 23S rRNA precursors are cleaved at sites that are consistent with production of the immediate precursors to the mature rRNAs. Substrate reactivity is independent of the distal box sequence, but is strongly dependent on the proximal box sequence. Structural studies have shown that a conserved glutamine (Q157) in the Aa-RNase III dsRNA-binding domain (dsRBD) directly interacts with a proximal box base pair. Aa-RNase III cleavage of the pre-16S substrate is blocked by the Q157A mutation, which reflects a loss of substrate binding affinity. Thus, a highly conserved dsRBD-substrate interaction plays an important role in substrate recognition by bacterial RNase III.

INTRODUCTION

The enzymatic cleavage of double-stranded (ds) RNA structures is an essential step in the maturation and decay of many eukaryotic and bacterial RNAs, and is a central participant in post-transcriptional gene silencing. Members of the ribonuclease III family are the primary agents of dsRNA processing, and are broadly conserved in Eukarya and Bacteria (1–6). The eukaryotic orthologs Dicer and Drosha function in the maturation of microRNAs which control mRNA translation, and Dicer also generates endogenous short interfering RNAs that participate in host defense and genome maintenance (5–7). Viral RNases III can counteract the host RNAi response (8), and also may have other functions in viral replication (9). RNase III polypeptides are components of trypanosomatid editosomes, and catalyze the endonucleolytic cleavages required for uridine insertion or deletion in pre-mRNA editing (10,11). Bacterial RNases III have a common role in the maturation of the 16S and 23S ribosomal RNAs (12,13), and also process diverse cellular, phage and plasmid RNAs. Bacterial RNase III controls antibiotic synthesis in *Streptomyces coelicolor* (14), supports virulence factor production in *Staphylococcus aureus* (15), and participates in phage strategies of infection (16,17). In contrast, RNase III is not commonly found in the Archaea. Whether RNase III family members function in a non-catalytic manner has not been definitively established, but a chloroplast RNase III polypeptide that is catalytically inactive functions as a chaperone for folding of a Group II intron (18).

RNase III family members are phosphodiesterases, and require a divalent metal cation for catalytic activity. Cleavage of the two phosphodiesters at double-helical target sites creates product ends with characteristic two-nucleotide, 3′-overhangs, and 5′-phosphomonoester, 3′-hydroxyl termini (19). Some bacterial RNase III substrates contain internal loops that limit cleavage to a single phosphodiester (20), while other structural motifs allow enzyme binding but block cleavage (21). Bacterial RNase III polypeptides generally consist of ~220 amino acids, and exhibit an N-terminal nuclease domain (NucD) that contains a set of highly conserved carboxylic acid residues that interact with the metal ions. A short linker connects the NucD to the C-terminal dsRNA-binding domain (dsRBD), containing a single copy of the

*To whom correspondence should be addressed. Tel: +1 215 204 9048; Fax: +1 215 204 1532; Email: anichol@temple.edu

conserved dsRNA-binding motif (Figure 1B). Dimerization of the NucD forms the active holoenzyme that contains two dsRBDs, both of which are needed for optimal activity (22). A recently characterized *Bacillus subtilis* RNase III ortholog ('Mini-III') that lacks the C-terminal dsRBD catalyzes formation of the 5′-end of 23S rRNA, with the assistance of ribosomal protein L3 (23,24).

Analyses of high-resolution structures of *A. aeolicus* (Aa)-RNase III, with and without bound dsRNA, have served to rationalize a large body of genetic and biochemical data on bacterial RNases III, especially that of *Escherichia coli* (Ec) RNase III, and also have provided insight on the mechanisms of eukaryotic family members including Dicer (25–30). Salient structural features of Aa-RNase III include (i) a subunit interface created by NucD dimerization that provides a dsRNA-binding valley; (ii) the symmetric positioning of the two catalytic sites that determines the characteristic 2-nt 3′-overhang product ends; (iii), two closely-positioned divalent

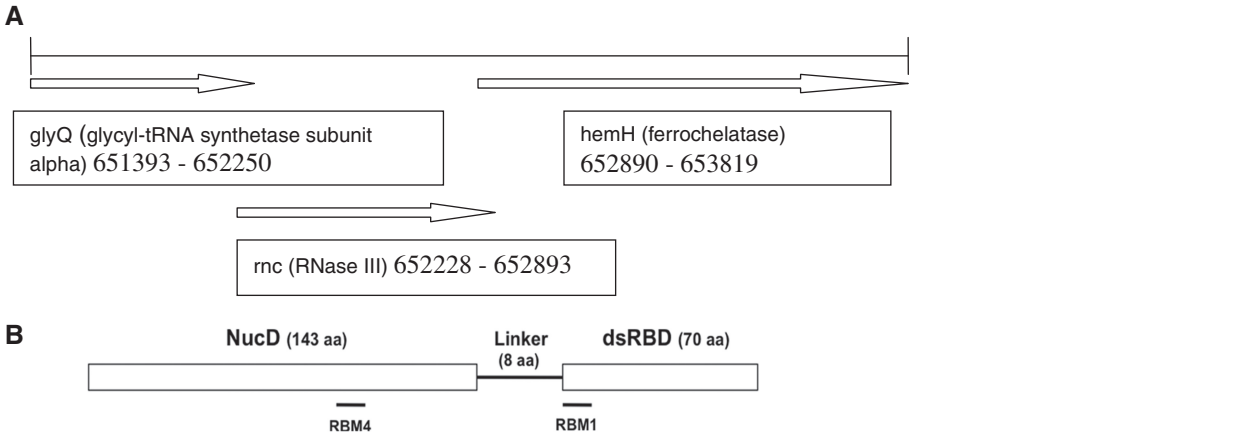

C

```
A. aeolicus            MKMLE QLEKKLGYTF KDKSLLEKAL THVSYS---- ------KKEH YETLEFLGDA   45
T. maritima         MNESERKIVE EFQKETGINF KNEELLFRAL CHSSYANEQN QAGRKD VES NEKLEFLGDA   59
M. tuberculosis        MIRSRQ PLLDALGVDL -PDELLSLAL THRSYAYENG ------GLPT NERLEFLGDA   49
E. coli              MNPIVIN RLQRKLGYTF NHQELLQQAL THRSAS---- ------SK-H NERLEFLGDS   46

                                                                        RBM4

A. aeolicus         LVNFFIVDLL VQYSPNKREG FLSPLKAYLI SEEFFNLLAQ KL---ELHKF IRIKRG--KI  100
T. maritimaa        VLELFVCEIL YKKYPEAEVG DLARVKSAAA SEEVLAMVSR KM---NLGKF LFLGKGEEKT  116
M. tuberculosis     VLGLTITDAL FHRHPDRSEG DLAKLRASVV NTQALADVAR RLCAEGLGVH VLLGRGEANT  109
E. coli             ILSYVIANAL YHRFPRVDEG DMSRMRATLV RGNTLAELAR EF---ELGEC LRLGPGELKS  103

                                                                  Linker

A. aeolicus         ----NETIIG DVFEALWAAV YIDSGRDANF TRELFYKLFK EDILSAIKEG RVKKD       151
T. maritima         GGRDRDSILA DAFEALLAAI YLDQ--GYEK IKELFEQEFE FYIEKIMK-G EMLFD       168
M. tuberculosis     GGADKSSILA DGMESLLGAI YLQH--GMEK AREVILRLFG PLLDAAPTLG AGL-D       155
E. coli             GGFRRESILA DTVEALIGGV FLDS--DIQT VEKLILNWYQ TRLDEI-SPG DKQKD       155

                    RBM1

A. aeolicus         YKTILQEITQ KRWKERPEYR LISVEGPHHK KKFIVEAKIK -EYRTL-GEG KSKKEAEQRA  209
T. maritima         YKTALQEIVQ SEHKVPPEYI LVRTEKNDGD RIFVVEVRVN GKTIAT-GKG RTKKEAEKEA  227
M. tuberculosis     WKTSLQELTA ARGLGAPSYL VTSTGPDHDK EFTAVVVVMD SEYGS--GVG RSKKEAEQKA  213
E. coli             PKTRLQEYLQ GRHLPLPTYL VVQVRGEAHD QEFTIHCQVS GLSEPVVGTG SSRRKAEQAA  215
                          *

A. aeolicus         AEELIKLLEE SE--------- 221
T. maritima         ARIAYEKLLK ERS-------- 240
M. tuberculosis     AAAAWKALEV LDNAMPGKTSA 234
E. coli             AEQALKKLEL E---------  226
```

NucD

dsRBD

Figure 1. Features of the *A. aeolicus* RNase III gene and polypeptide. (**A**) Diagram of the *A. aeolicus* chromosomal region that carries the RNase III (rnc) gene. The RNase III open-reading frame (ORF) exhibits a 22-nt overlap with the ORF for the α-subunit of glycyl-tRNA synthetase, suggesting coupled expression of the two cistrons. (**B**) Domain structure of the Aa-RNase III polypeptide. Indicated are the N-terminal nuclease domain (NucD), linker, C-terminal dsRBD and the positions of RNA-binding motifs 1 and 4 (RBM1 and RBM4) that interact with the substrate proximal box and distal box, respectively (28,29) (see also 'Results' section). (**C**) Sequence alignment of selected bacterial RNase III orthologs. Shown are the positions of the NucD, linker, dsRBD, RBM1 and RBM4. The asterisk indicates the conserved glutamine in RBM1 (Q157 in Aa-RNase III) that was mutated to alanine (see 'Results' section).

metal ions in each catalytic site; and (iv) a flexible linker that confers positional mobility on the dsRBD (25–29). In contrast to the extensive structural information, the biochemical behavior of Aa-RNase III and the structures and reactivities of its cognate substrates have not been described. Such information in conjunction with the structural data would provide insight on the fundamental steps in the catalysis of dsRNA cleavage. We present here a biochemical analysis of Aa-RNase III, including the demonstration of its robust thermostability, the dependence of catalytic activity on divalent metal cation type and concentration, and the effects of salt concentration and pH. We use small RNA hairpins based on the double-stranded stems associated with the Aquifex 16S and 23S rRNA precursors to analyze the dependence of processing reactivity on base pair sequence, and to identify a conserved, functionally important RNase III–substrate interaction.

MATERIALS AND METHODS

Materials

Water was deionized and distilled. Chemicals and reagents were molecular biology grade and were obtained either from Sigma-Aldrich or ThermoFisher. Standardized 1 M solutions of $MgCl_2$ and $MnCl_2$ were purchased from Sigma-Aldrich. Ribonucleoside 5′-triphosphates were obtained from Roche Molecular Biochemicals. [γ-^{32}P]ATP (3000 Ci/mmol), [α-^{32}P]UTP (3000 Ci/mmol) and [5′-^{32}P]pCp (3000 Ci/mmol) were purchased from Perkin-Elmer. Bacteriophage T7 RNA polymerase (31) and *E. coli* RNase III (32) were purified as described. The single chromosomal gene (*rnc*) encoding Aa-RNase III (Figure 1A) was amplified by PCR from a sample of *A. aeolicus* DNA (a generous gift of R. Huber), and cloned into the NdeI and BamHI sites of plasmid pET-15b (Novagen) as described (33). Production of recombinant Aa-RNase III used the *E. coli* expression strain BL21(DE3)*rnc*105*rec*A (33) that carries an inactivating mutation (*rnc105*) of the chromosomal RNase III gene. Cell cultures were grown at 37°C, and protein expression induced by IPTG (1 mM). Aa-RNase III was purified from the soluble portion of sonicated cell extracts using Ni^{2+} affinity chromatography (32,33). Alternatively, the protein present in the inclusion body of cell lysates was solubilized by including 6 M urea in the sonication buffer, and the enzyme purified from the clarified sonicate by affinity chromatography (32). The Q157A mutation was introduced into the cloned Aa-RNase III gene by standard procedures (QuikChange Kit, Agilent Technologies), and the Aa-RNase III Q157A mutant was purified as described above. To determine whether the N-terminal $(His)_6$ tag influenced catalytic activity, it was removed by treatment with soluble recombinant bovine thrombin (Novagen), followed by gel filtration chromatography on a SuperDex 75 column (Akta Explorer FPLC system). Time-course cleavage assays using ^{32}P-labeled RNA revealed no significant differences in cleavage rate between the two forms of the enzyme (Supplementary Figure S1). Experiments in this study used $(His)_6$-tagged Aa-RNase III, and all reported concentrations refer to the homodimer concentration.

RNA synthesis

Oligodeoxynucleotides used as transcription templates were synthesized by Invitrogen and were provided in deprotected, desalted form. DNAs were further purified by denaturing gel electrophoresis and stored at −20°C in 10 mM Tris–HCl (pH 8), 1 mM EDTA. Internally ^{32}P-labeled RNAs were synthesized and purified by gel electrophoresis as described (32,34). The specific activity of the UTP in the transcription reactions was 300 Ci/mol. For 5′-^{32}P-labeling, RNA was treated first with shrimp alkaline phosphatase (Roche Biochemicals), then treated with T4 polynucleotide kinase (New England BioLabs) and [γ-^{32}P]ATP. The labeled RNA was purified by electrophoresis in a 15% polyacrylamide gel containing 6 M urea, then extracted, ethanol precipitated, and stored at −20°C in 10 mM Tris–HCl (pH 7.5), 1 mM EDTA as described (32). Alternatively, RNA was 3′-^{32}P labeled using T4 RNA ligase (New England Biolabs) and [5′-^{32}P]pCp as described (35), and purified by denaturing gel electrophoresis.

RNA cleavage assay

RNA cleavage assays were performed using a standard reaction buffer, established as described below, that consisted of 50 mM NaCl, 10 mM $MgCl_2$ and 30 mM Tris–HCl (pH 8). Reaction temperatures were in the experimentally convenient range of 40–45°C, which represents the lower end of the optimum temperature range for the enzyme (*vide infra*). Prior to use, RNA was heated at 100°C for 2 min, then placed on ice. Aa-RNase III was pre-incubated at the assay temperature for 1 min prior to addition to the reaction, and, as specified in the appropriate figure legends, either Mg^{2+} or RNase III was added last to initiate the reaction. Other specific conditions for the assays, including enzyme and RNA concentrations, are provided in the figure legends. Reactions were stopped by the addition of an equal volume of loading dye containing 40 mM EDTA (32), and aliquots were analyzed by electrophoresis in a 15% polyacrylamide gel containing 7 M urea in TBE buffer. Reactions were visualized by phosphorimaging (Typhoon 9400). Initial rates of substrate cleavage were determined as described (33), under conditions of substrate excess, and using reaction times where less than ~20% of the substrate was cleaved. Assays were performed in duplicate, with maximum error less than ~20%. Determination of kinetic parameters (K_m, V_{max}) involved generation (Kaleidagraph v.4) of the best-fit curve to a Michaelis–Menten kinetic scheme.

RNA binding assay

Gel shift assays of RNA binding to Aa-RNase III used 5′-^{32}P-labeled RNA (see above). Prior to use, the RNA was heated in 10 mM Tris–HCl (pH 7.5), 1 mM EDTA at 100°C for 2 min, then placed on ice. Binding reactions (20 µl) contained RNA (~8000 d.p.m.; ~1–2 fmol) in

buffer consisting of 250 mM potassium glutamate, 5 mM $CaCl_2$, 5 mM spermidine, 30 mM Tris–HCl (pH 8.0), 0.1 mM DTT and 5% (v/v) glycerol. Following addition of Aa-RNase III at the specified concentration, the reactions were incubated at ~22°C for 10–20 min, then electrophoresed (10 V/cm) at room temperature in an 8% polyacrylamide gel (15 cm, 80:1 acrylamide:bisacrylamide) containing 45 mM Tris, 45 mM Boric acid, 1 mM EDTA, 5 mM $CaCl_2$ and 2.5% (v/v) glycerol. The electrophoresis buffer was identical to the polyacrylamide gel buffer, and the gel was electrophoresed (10 V/cm) for 30 min prior to sample addition. To track the progress of electrophoresis, side lanes contained bromophenol blue (0.04% w/v) in binding reaction buffer. Reactions were visualized by phosphorimaging, and the fraction of substrate bound was determined as described (36). Some dissociation of RNA–protein complexes occurred during electrophoresis, causing a 'trail' of ^{32}P radioactivity extending up from the free (unbound) RNA. This behavior has been noted elsewhere (37), and was taken into account as described (37) in determining the fraction of substrate bound. Dissociation constants (K_d) of the RNA-protein complexes were calculated by determining the slope of the best-fit line to the reciprocal of the fraction of RNA bound *versus* the reciprocal of the protein concentration (36). Reactions were performed in duplicate, and average values are reported with maximum error less than ~20%.

RESULTS

Divalent metal ion dependence of Aa-RNase III catalytic activity

Structural (29) and biochemical (38) studies of Aa-RNase III and Ec-RNase III, respectively, have identified a two-metal-ion catalytic mechanism. Since Ec-RNase III can use several different divalent metal ions, with Mg^{2+} supporting optimal activity (19), it was of interest to determine the metal ion dependence of Aa-RNase III. We examined the ability of Mg^{2+}, Mn^{2+}, Ni^{2+}, Co^{2+} and Ca^{2+} to support Aa-RNase III catalytic activity. The substrate, Aa-23S[hp] RNA (Figure 5C), is characterized in more detail below. Short reaction times were applied to limit the extent of the reaction, allowing more accurate assessment of the metal ion dependence. Cleavage assays (Figure 2A and B) show that both Mg^{2+} and Mn^{2+} support catalytic activity to comparable extents, and the internally ^{32}P-labeled RNA cleavage patterns indicate that the same scissile bond is selected. However, higher Mn^{2+} concentrations lead to several additional products (Figure 2B). Quantitative analysis (Figure 2C) shows that maximal activity is achieved at a ~4 mM concentration of either Mg^{2+} or Mn^{2+}, while Co^{2+} supports only minor levels of activity. Neither Ni^{2+} nor Ca^{2+} support catalytic activity over the concentration range examined (data not shown). Based on these results Mg^{2+} (10 mM) was selected as a standard reaction component.

Salt and pH dependence of Aa-RNase III catalytic activity

Monovalent cations affect Ec-RNase III activity *in vitro*. At salt concentrations ~100–150 mM, Ec-RNase III exhibits optimal activity and specificity, while at lower salt concentrations, additional sites are cleaved (39). To assess the effect of salt type and concentration on Aa-RNase III activity, substrate cleavage assays were performed using a range of concentrations of Na^+, K^+ or NH_4^+ (as the chloride salts), and in the presence of 10 mM Mg^{2+}. These assays used Aa-16S[hp] RNA (Figure 5B), which is characterized in more detail below. The results are summarized in Figure 3A, where it is observed that Aa-RNase III catalytic activity generally increases with increasing salt, reaching a maximum at ~50 mM Na^+, ~50 mM K^+ or ~25 mM NH_4^+, with higher concentrations of each species causing a progressive reduction in activity. The results demonstrate the absence of a strong preference for a specific salt, and that there is no salt concentration-dependent change in the cleavage pattern. The pH dependence of Aa-RNase III catalytic activity was determined by measuring the extent of Aa-16S[hp] RNA cleavage at pH values between 6 and 9, and in the presence of 10 mM Mg^{2+} and 50 mM Na^+. The fraction of substrate cleaved as a function of pH is shown in Figure 3B, which reveals a transition to maximal activity between pH 6 and 9. The shape of the transition suggests the generation of a more active form of the enzyme by deprotonation of one or more groups with an apparent pK of ~7 (see also 'Discussion' section). Based on these results, NaCl (50 mM) and pH 8 were incorporated as standard reaction components.

Thermostability of Aa-RNase III catalytic activity

We determined the temperature dependence of Aa-RNase III catalytic activity using Aa-16S[hp] RNA as substrate. For comparison, we assessed in parallel the temperature dependence of Ec-RNase III, using the same substrate. Reactions were initiated by adding RNase III at the specified temperature, then quenched with excess EDTA, and the fraction of substrate cleaved determined. To minimize temperature-dependent changes in buffer pK, the pH was adjusted to 8 at each temperature used in the assay. Figure 4A and B show phosphorimages of the experiments with Aa-RNase III and Ec-RNase III, respectively, and the data are graphically summarized in Figure 4C. Aa-RNase III activity increases from 35°C, reaching a maximum at ~70°C, and with significant activity exhibited up to ~85°C. In contrast, Ec-RNase III exhibits a lower temperature range of activity, with essentially all activity lost by ~60–65°C. We conclude that Aa-RNase III catalytic activity exhibits substantial thermostability, compared to Ec-RNase III. The possible sources of the thermostability are addressed in the 'Discussion' section.

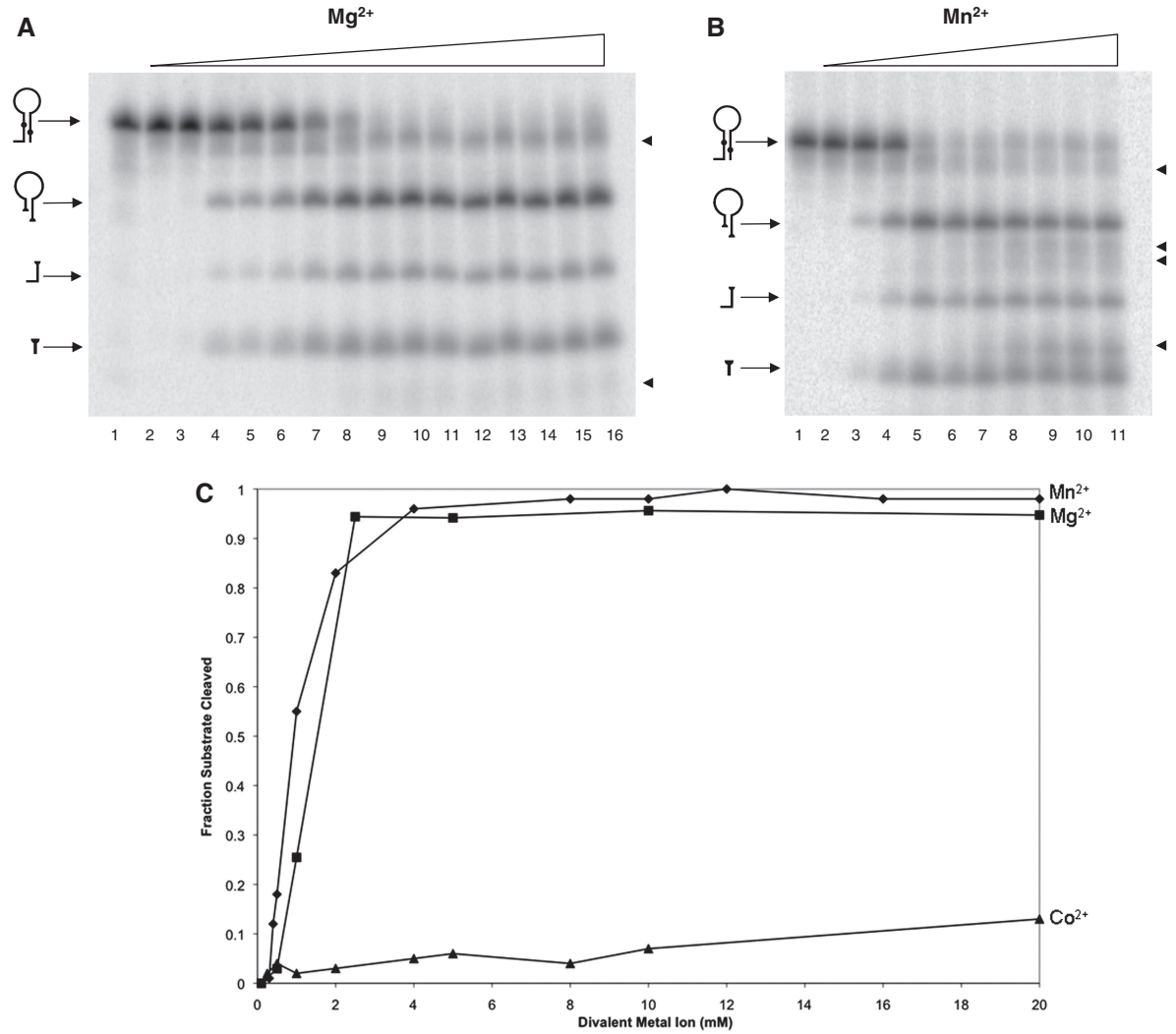

Figure 2. Divalent metal ion dependence of Aa-RNase III catalytic activity. Internally ^{32}P-labeled Aa-23S[hp] RNA (100 nM) was incubated with Aa-RNase III (30 nM) at 45°C for 2 min in the standard reaction buffer, containing the specified divalent metal ion at the indicated concentration. Reactions were stopped with EDTA and aliquots electrophoresed in a denaturing 15% polyacrylamide gel as described in 'Materials and Methods' section. Reactions were visualized by phosphorimaging. (**A**) Dependence of catalytic activity on the Mg^{2+} concentration. Lanes 2–16 show reactions using $MgCl_2$ concentrations of 0.1, 0.2, 0.3, 0.4, 0.5, 1, 2, 4, 8, 10, 12, 16, 20, 30 and 50 mM, respectively. Lane 1 shows a 2-min reaction in the absence of Mg^{2+}. The positions of the substrate, and the three products of cleavage are indicated by the figures on the left. The arrowhead on the upper right indicates a cleavage-resistant species, and may represent an unreactive substrate conformation. The arrowhead on the lower right indicates a low-level product appearing at higher Mg^{2+} concentrations. (**B**) Dependence of catalytic activity on the Mn^{2+} concentration. Lanes 2–11 show reactions using $MnCl_2$ concentrations of 0.1, 0.5, 1.0, 2.5, 5, 10, 20, 40, 80, and 100 mM, respectively. Lane 1 represents a 2-min reaction in the absence of Mn^{2+}. The figures on the left indicate the positions of substrate and the three products. The arrowheads on the right side of the gel indicate low-level cleavage products generated at higher Mn^{2+} concentrations. (**C**) Graphic analysis of the divalent metal ion dependence of catalytic activity. The fraction of Aa-23S[hp] RNA cleaved was plotted as a function of divalent metal ion concentration. The Mg^{2+} dependence is indicated by squares, Mn^{2+} by diamonds and Co^{2+} by triangles. Neither Ca^{2+} nor Ni^{2+} supported a detectable level of catalytic activity over the tested concentrations (data not shown).

Site-specific cleavage of RNA hairpins based on the Aquifex pre-16S and pre-23S rRNA processing stems

The *A. aeolicus* chromosome contains two regions that encode the three ribosomal RNAs in the standard order, 16S–23S–5S (Figure 5A) (40,41). The sequences that flank the 16S and 23S rRNAs are predicted to pair, forming ~33 and ~44 bp stems, respectively (Figure 5B and C) (42). Based on studies of Ec-RNase III action on the cognate rRNA precursors (12,13,43,44), these stem structures also represent likely targets for Aa-RNase III. The Aquifex pre-16S and pre-23S stem sequences were incorporated into small hairpin RNAs, Aa-16S[hp] RNA and Aa-23S[hp] RNA (Figure 5B and C). Time course assays of the internally ^{32}P-labeled RNAs (Figure 6A) reveal that each RNA is cleaved in a site-specific manner, yielding three products whose sizes are consistent with the recognition of a single target site containing two scissile bonds. The two RNAs exhibit unequal reactivities, as Aa-16S[hp] RNA is cleaved at a significantly slower rate than Aa-23S[hp] RNA. The cleavage sites in each RNA were mapped by comparison of the gel electrophoretic mobilities of the products of Aa-RNase III cleavage of

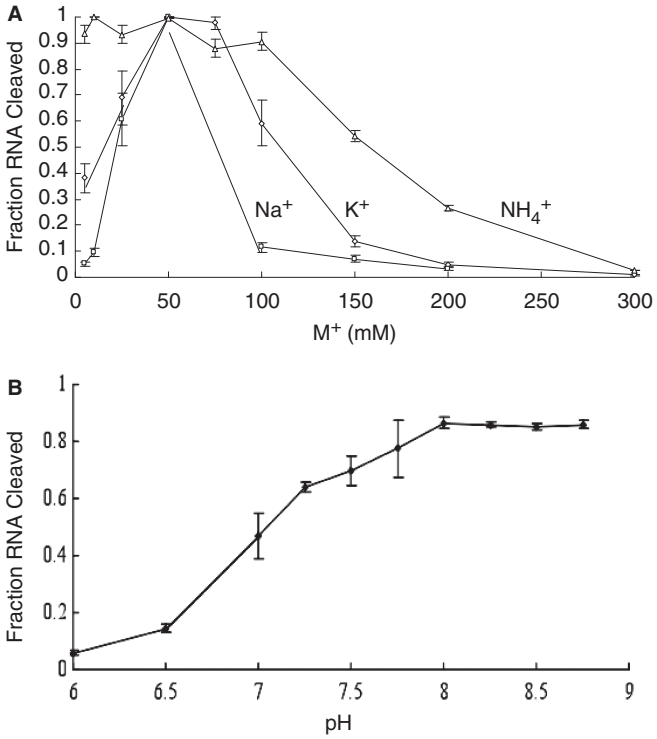

Figure 3. Salt and pH dependence of Aa-RNase III catalytic activity. (**A**) Salt dependence of catalytic activity. Cleavage reactions were performed in duplicate using internally ^{32}P-labeled Aa-16S[hp] RNA (100 nM) and Aa-RNase III (20 nM), in buffer containing 10 mM Mg^{2+}, 30 mM Tris–HCl (pH 8) and the specified salt at the indicated concentrations. Reactions were incubated at 40°C for 1 min, then stopped by excess EDTA and aliquots analyzed by gel electrophoresis as described in 'Materials and Methods' section. The fraction of substrate cleaved was determined and plotted as a function of salt concentration. Symbols represent the average values, with maximum errors shown. Open triangles represent NH_4^+ concentrations, open squares represent Na^+ concentrations, and open diamonds represent K^+ concentrations. (**B**) pH dependence of catalytic activity. Reactions were performed in duplicate, using internally ^{32}P-labeled Aa-16S[hp] RNA (100 nM), Aa-RNase III (20 nM), 50 mM NaCl, 10 mM $MgCl_2$ and 30 mM Tris–HCl adjusted to the indicated pH. Reactions were incubated for 1 min at 40°C, then quenched by EDTA and aliquots analyzed by electrophoresis as described in 'Materials and Methods' section. The fraction of substrate cleaved was determined, and plotted as a function of pH. Maximum errors are shown for the averaged data points. The differing activities in the absence of added salt represent variation in this specific condition, between experiments performed on separate occasions, but do not otherwise affect interpretation of the overall salt concentration dependencies.

5′-^{32}P or 3′-^{32}P-labeled RNA with the products of either partial cleavage by P1 nuclease, or incubation in alkaline buffer. The results (Supplementary Figure S2) show that the cleavage sites (shown by the arrows in Figure 5B and C) occupy equivalent positions in each hairpin. Their placement is consistent with a role for Aa-RNase III in creating the immediate precursors to the mature 16S and 23S rRNAs.

Gel mobility shift assays were performed to assess whether target site selectivity and processing efficiency can be related to specific complex formation and stability. Ca^{2+} was included in the reaction buffer, which was shown for Ec-RNase III to stabilize the RNA–protein complex (45), but which does not support Aa-RNase III catalytic activity (see above). Figure 6B and C show that each RNA binds Aa-RNase III to form a complex with reduced electrophoretic mobility. The observation of a single complex is in accord with a single target site for cleavage for each RNA. The K_d value for each complex was determined by quantitative analysis of the gel shift assays, and are 3.5 μM for the Aa-RNase III•16S[hp] RNA complex, and 72 nM for the Aa-RNase III•23S[hp] RNA complex (Supplementary Figure S3). The larger K_d value for the Aa-16S[hp] RNA complex is reflected in the comparatively lower reactivity of the RNA (Figure 6A).

Base pair sequence control of pre-16S rRNA substrate reactivity

The reactivities of Ec-RNase III substrates are determined in part by sequences within the proximal box (pb) and distal box (db) (46,47). Crystallographic studies of Aa-RNase III bound to cleaved hairpin RNAs (28,29) show that the pb and db, as well as an additional 2-bp segment termed the middle box (mb) (28), are sites of protein contact. The structural data suggest that the bp sequences within the boxes may influence reactivity. To examine this possibility, a minimal hairpin substrate (Aa-16S[μ-hp] RNA; Figure 7A) was prepared according to a previous strategy (47). The 3′-end of Aa-16S[μ-hp] RNA corresponds to the 3′-end-proximal cleavage site of Aa-16S[hp] RNA, and retains the 5′-end-proximal cleavage site. While full-length Aa-16S[hp] RNA (Figure 5B), which contains an A–C pair adjacent to the 3′ cleavage site, is reactive (see above), the presence of this base mismatch in Aa-16S[μ-hp] RNA inhibited cleavage (data not shown). Therefore, the A–C pair was changed to an A–U pair to provide a reactive version of Aa-16S[μ-hp] RNA. A time course assay of cleavage (Figure 7B) reveals that the RNA is cleaved at a single site. Since the longer product co-migrates with the largest product of Aa-16S[hp] RNA cleavage, which is the shortened, processed hairpin, the Aa-16S[μ-hp] RNA cleavage site corresponds to the 5′-end-proximal cleavage site of Aa-16S[hp] RNA. The K_m and k_{cat} values were determined by measuring the initial rate as a function of substrate concentration, and fitting the rate dependence on substrate concentration to a Michaelis–Menten kinetic scheme (Supplementary Figure S4). For Aa-[16S[μ-hp] RNA, the K_m is 98 nM and the k_{cat} is 2.7 min^{-1}, corresponding to a catalytic efficiency (k_{cat}/K_m) of $2.8 \times 10^7\ min^{-1}\ M^{-1}$ (40°C).

Next, single base-pair substitutions were introduced in Aa-16S[μ-hp] RNA at each position between the cleavage site and the tetraloop. An additional variant possessed an altered tetraloop sequence. The initial rates of cleavage were measured under conditions of excess substrate, and the relative reactivities were calculated as the ratio of the initial rate of cleavage of a variant to that of Aa-16S[μ-hp] RNA. The relative reactivities are provided below the bp substitutions in Figure 7A. Substitutions having significant effects were identified as those that reduced the relative reactivity to <0.5. Based on this criterion, the greatest inhibitory effects were seen with specific

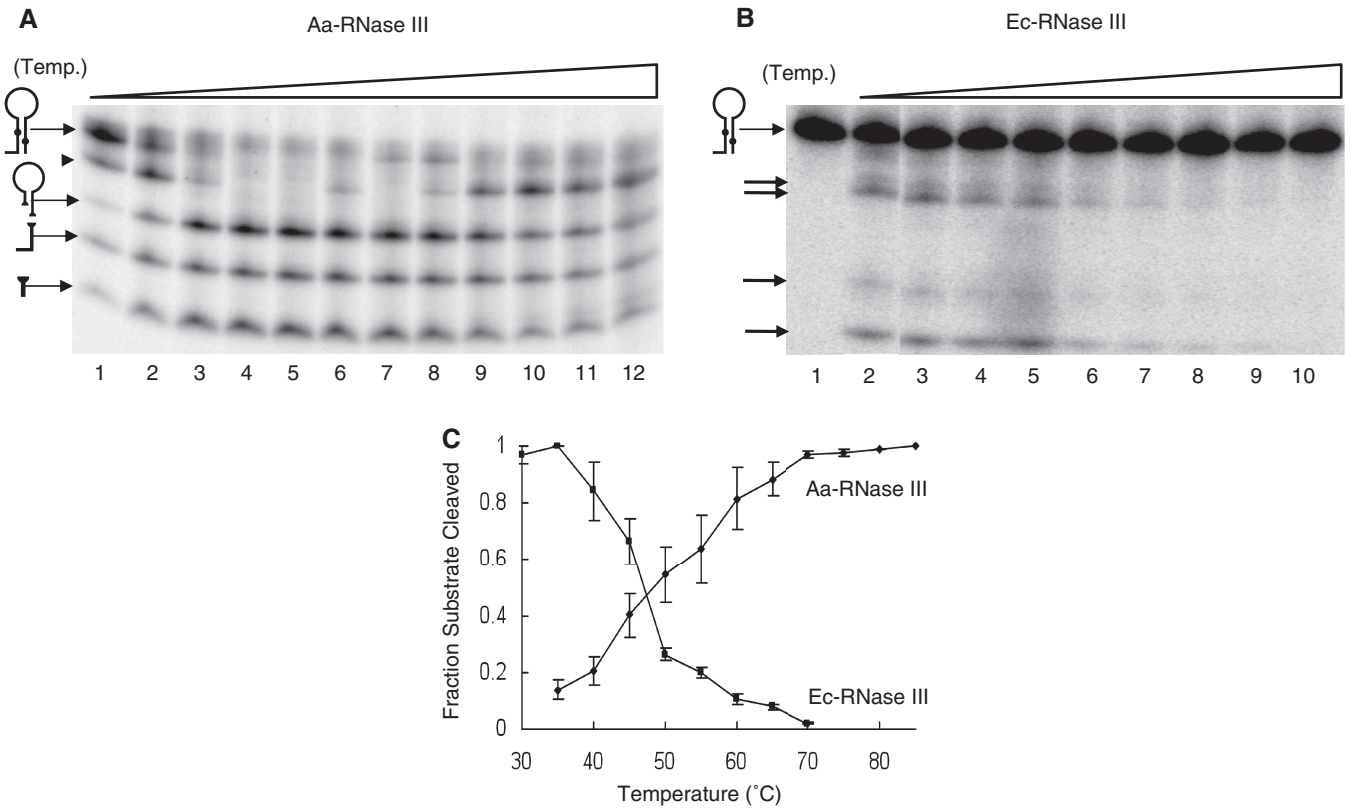

Figure 4. Temperature dependence of Aa-RNase III catalytic activity. (**A**) Temperature dependence of Aa-RNase III cleavage of Aa-16S[hp] RNA. Reactions were performed in duplicate, and involved internally ^{32}P-labeled Aa-16S[hp] RNA (100 nM) and Aa-RNase III (20 nM) in 50 mM NaCl, 10 mM $MgCl_2$ and 30 mM Tris–HCl (pH 8.0). The Tris buffer was adjusted to pH 8 at each temperature used in the experiment. Reactions were performed for 1 min at the specified temperature, then stopped by EDTA and aliquots electrophoresed in a 15% polyacrylamide gel containing 7M urea. Lanes 1–12 show reactions performed at temperatures of 30, 35, 40, 45, 50, 55, 60, 65, 70, 75, 80 and 85°C. The figures on the left indicate the positions of the substrate and the three products. The arrowhead indicates the product of cleavage of only one of the two scissile phosphodiesters. (**B**) Temperature dependence of Ec-RNase III cleavage of Aa-16S[hp] RNA. Experimental conditions were the same as in (A). Lanes 2–10 represent reaction temperatures of 30, 35, 40, 45, 50, 55, 60, 65 and 70°C. Lane 1 represents RNA directly subjected to electrophoresis without prior incubation. The position of Aa-16S[hp] RNA is indicated, along with cleavage products that differ in size from those produced by Aa-RNase III, as shown in (A). (**C**) Graphic comparison of the temperature dependence of the catalytic activities of Aa-RNase III and Ec-RNase III. Points represent average values of duplicate experiments, and maximum errors are shown.

substitutions within the proximal box. Thus, an AU→CG or GC bp change at pb position 2 or 4 caused a 10-fold reduction in reactivity (Figure 7C and D, respectively), while a GC→UA substitution at pb position 3 caused a 5-fold reduction in reactivity (Figure 7A). In contrast, substitutions in the db had negligible effects on reactivity, while substitutions within the mb had, at most, only moderate effects (Figure 7A). There also is no strict dependence of reactivity on the tetraloop sequence (Figure 7A). We conclude that the pb is the primary determinant of reactivity for the Aa-RNase III pre-rRNA substrate, with pb positions 2, 3 and 4 playing a dominant role. The consensus pb sequence is shown in the inset in Figure 7, and the functional importance of the bp at pb position 2 is analyzed further below.

A conserved glutamine in the dsRBD that contacts a proximal box base pair is important for substrate binding

A conserved glutamine within the N-terminal portion of the dsRBD (Figure 1C) is invariant among 100 examined bacterial RNase III sequences (29). A crystallographic analysis of Aa-RNase III bound to a cleaved RNA (28) showed that the side chain of Q157 is engaged in two hydrogen bonds with the U of the UA bp at pb position 2 (Figure 8C, left). One hydrogen bond involves the Q157 carboxamide oxygen atom and uridine 2′-OH group, while the other hydrogen bond involves the carboxamide amine group and the uracil O2 atom. The strong conservation of the glutamine and the dependence of reactivity on the identity of the bp at pb position 2 (see above) suggest a functionally important interaction. To assess this possibility, Q157 was changed to alanine. The Q157A mutation did not affect folding or structure in a significant manner, since (i) the mutant protein was efficiently overexpressed in soluble form, and (ii) the circular dichroism spectrum of the protein matches that of Aa-RNase III (Supplementary Figure S5). Time-course cleavage assays (Figure 8A) show that the Q157A mutant does not exhibit detectable catalytic activity, under conditions where Aa-RNase III efficiently processes Aa-16S[hp] RNA. A gel shift assay (Figure 8B) reveals that the inactivity of the Q157A mutant reflects a defect in substrate binding, to an

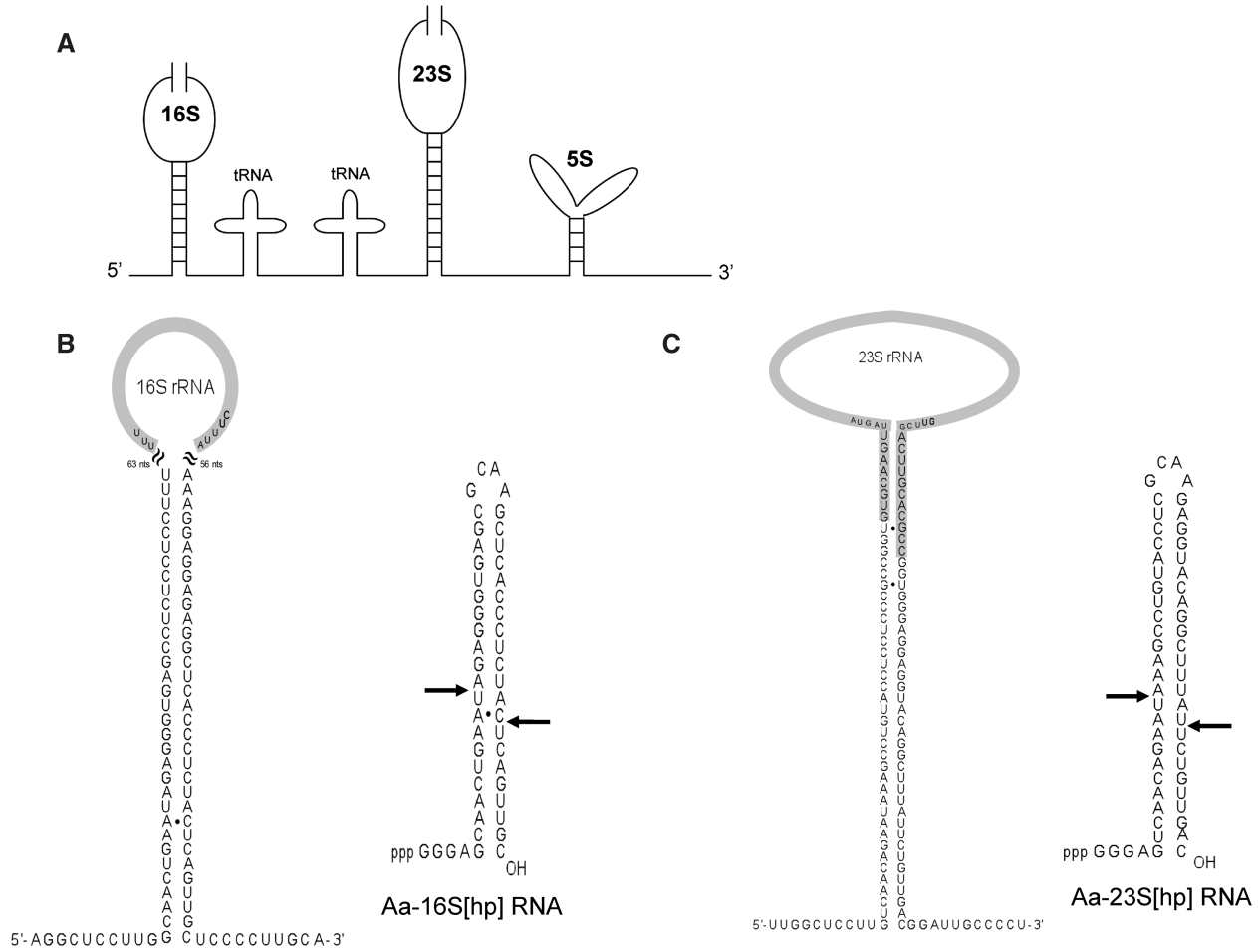

Figure 5. Structures of the Aquifex pre-16S and pre-23S rRNA processing stems and corresponding hairpin substrates. (**A**) Putative primary transcript of one of the two *A. aeolicus* 16S–23S–5S genetic loci, emphasizing the base-paired stem structures associated with the 16S and 23S rRNA sequences. (**B**) Sequence and proposed structure of the 16S pre-rRNA stem (left) and the corresponding hairpin substrate, Aa-16S[hp] RNA (right). Arrows indicate the Aa-RNase III cleavage sites, which were mapped as described (see 'Results' section, and Supplementary Data, Figure S2). (**C**) Sequence and proposed structure of the 23S pre-rRNA stem (left) and corresponding hairpin substrate, Aa-23S[hp] RNA (right). In the processing stems, the nucleotide sequences within the mature rRNAs are shown in smaller size. Arrows indicate the Aa-RNase III cleavage sites (see 'Results' section, and Supplementary Data, Figure S2).

extent that the K_d of the complex was too large be determined in this manner. We conclude that the interaction of Q157 with the bp at pb position 2 is important for substrate binding.

DISCUSSION

This study has described the biochemical properties of *Aquifex aeolicus* RNase III and the reactivities of hairpin substrates based on the cognate pre-16S and pre-23S rRNA processing stems. Aa-RNase III catalytic activity is supported by either Mn^{2+} or Mg^{2+} with comparable efficiency. In contrast to Ec-RNase III (38,48), higher Mn^{2+} concentrations are not inhibitory. Regarding this difference it has been proposed that Mn^{2+} occupancy of a site near the two catalytic metal sites in Ec-RNase III inhibits product release (49). If this site also exists in Aa-RNase III [for evidence, see (29,50)], then its occupancy by Mn^{2+} is not inhibitory. A salt concentration optimum in the range of ~50 mM was observed, with increasing concentrations causing inhibition, perhaps reflecting ion competition with RNA for enzyme binding. Nonetheless, salt concentrations up to ~200 mM still allow reasonably efficient cleavage of either substrate at 45°C (Figure 6A). The pH dependence indicates that maximal activity requires the conjugate base forms of one or more enzyme groups. If the rate-limiting step for Aa-RNase III processing activity under steady-state conditions is associated with product release, as is the case with Ec-RNase III (51), then deprotonation may optimize this step.

Aa-RNase III exhibits a robust thermostability, with maximal activity achieved by ~70°C, and retained at temperatures approaching 90°C. In considering the sources of thermostability, it has been noted that the Charged-*versus*-Polar bias (C*v*P-bias) in the amino acid compositions of thermophile proteins is larger than that for mesophile proteins (52,53). The greater C*v*P-bias values reflect a preference for charged residues that can form salt bridges,

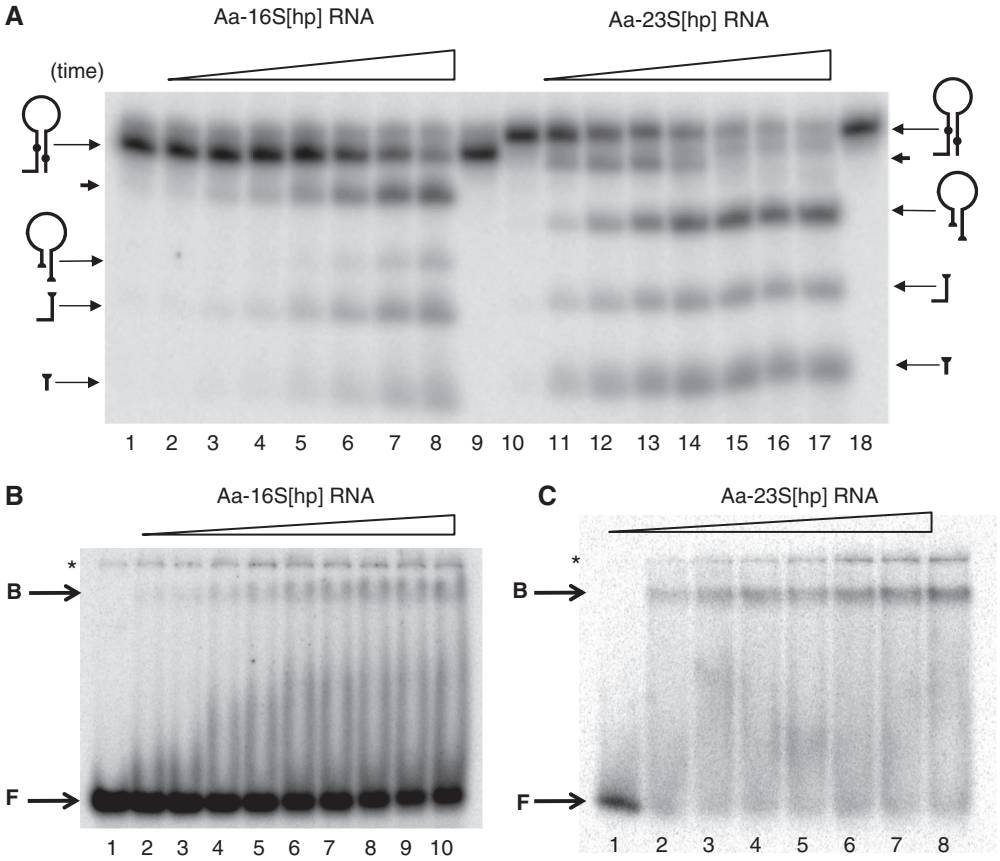

Figure 6. Reactivities and binding affinities of small hairpin RNAs based on the pre-16S and pre-23S rRNA processing stems. (**A**) Time course for Aa-RNase III cleavage of Aa-16S[hp] RNA and Aa-23S[hp] RNA. Internally ^{32}P-labeled Aa-16S[hp] RNA (400 nM) or Aa-23S[hp] RNA (200 nM) were combined with Aa-RNase III (30 nM) and incubated at 45°C in buffer consisting of 200 mM NaCl, 2 mM $MgCl_2$, 30 mM Tris–HCl (pH 8). The higher salt concentration used in this experiment reduced the reaction rate at 45°C (see Figure 3A), but did not alter the pattern of cleavage. Aliquots were combined with EDTA at the specified times and electrophoresed in a denaturing 15% polyacrylamide gel (see 'Materials and Methods' section). Lanes 2–8 and lanes 11–17 show reaction times of 0, 0.5, 1, 2, 4, 8 and 16 min for Aa-16S[hp] RNA and Aa-23S[hp] RNA, respectively. Lanes 1 and 10 represent complete reactions that were assembled then immediately quenched with excess EDTA. Lanes 9 and 18 represent 16-min reactions with Aa-6S[hp] RNA and Aa-23S[hp] RNA, respectively, that were otherwise complete, but lacked Mg^{2+}. Icons indicate the identities of the specific products. The short arrow indicates the product of cleavage of one of the two scissile bonds. (**B**) Gel shift assay of Aa-RNase III binding to Aa-16S[hp] RNA. 5′-^{32}P-labeled RNA (10^4 d.p.m.) was incubated with the specified amount of Aa-RNase III (see below) in binding buffer (see 'Materials and Methods' section) and electrophoresed in an 8% polyacrylamide gel containing 0.5× TBE buffer, 5 mM $CaCl_2$ and 2.5% (*v*/*v*) glycerol, also as described in 'Materials and Methods' section. Lanes 1–10 represent binding reactions containing 0, 10, 25, 50, 75, 100, 150, 200, 300 and 400 nM concentrations of Aa-RNase III, respectively. 'F' and 'B' indicate the positions of free and protein-bound forms of the RNA, respectively. The asterisk indicates the origin of electrophoresis. (**C**) Gel shift assay of Aa-RNase III binding to 5′-^{32}P-labeled Aa-23S[hp] RNA. Reactions were performed and electrophoresis carried out as described in 'Materials and Methods' section. Lanes 1–8 show reactions containing 0, 50, 75, 100, 150, 200, 250 and 300 nM Aa-RNase III (dimer concentration), respectively. Reactions were quantitated as described in 'Materials and Methods' section, and as shown in Supplementary Figure 3S, with the K_d values provided in the text (see 'Results' section). 'F' and 'B' indicate positions of free and bound forms of the RNA, respectively. The asterisk indicates the origin of electrophoresis.

as well as a preference for Glu/Asp instead of Gln/Asn that contain thermolabile carboxamide groups (52,53). For Aa-RNase III, the calculated C*v*P-bias is 22.2, while that for Ec-RNase III is 6.2. These values can be compared to the average C*v*P-bias values of 15.41 and 2.63 for Aa and Ec proteins, respectively (52,53). It may be concluded that the C*v*P-bias contributes to Aa-RNase III thermostability. A similar correlation between CvP-bias and thermostable catalytic activity was noted for *Thermotoga maritima* RNase III (54). Another contributor to thermostability is contact order (CO), which is a measure of structural compactness due to an increased density of non-nearest neighbor interactions (55–57). The calculated CO for the Aa-RNase III NucD (PDB: 1I4S) is 14.7 (relative CO, 0.10), while the CO for the RNase III NucD from the mesophile *Mycobacterium tuberculosis* (PDB: 2A11) is 14.3 (relative contact order, 0.09). The relative CO value for Aa-RNase III is only slightly higher than that of Mt-RNase III, so it can be concluded that CO is not a primary contributor to Aa-RNase III thermostability.

Functional implications of the site-specific cleavage of the Aquifex 16S and 23S pre-rRNA hairpins

The Aquifex pre-16S and pre-23S processing stems exhibit the greatest lengths and predicted thermodynamic stabilities among an examined set of bacterial pre-rRNA

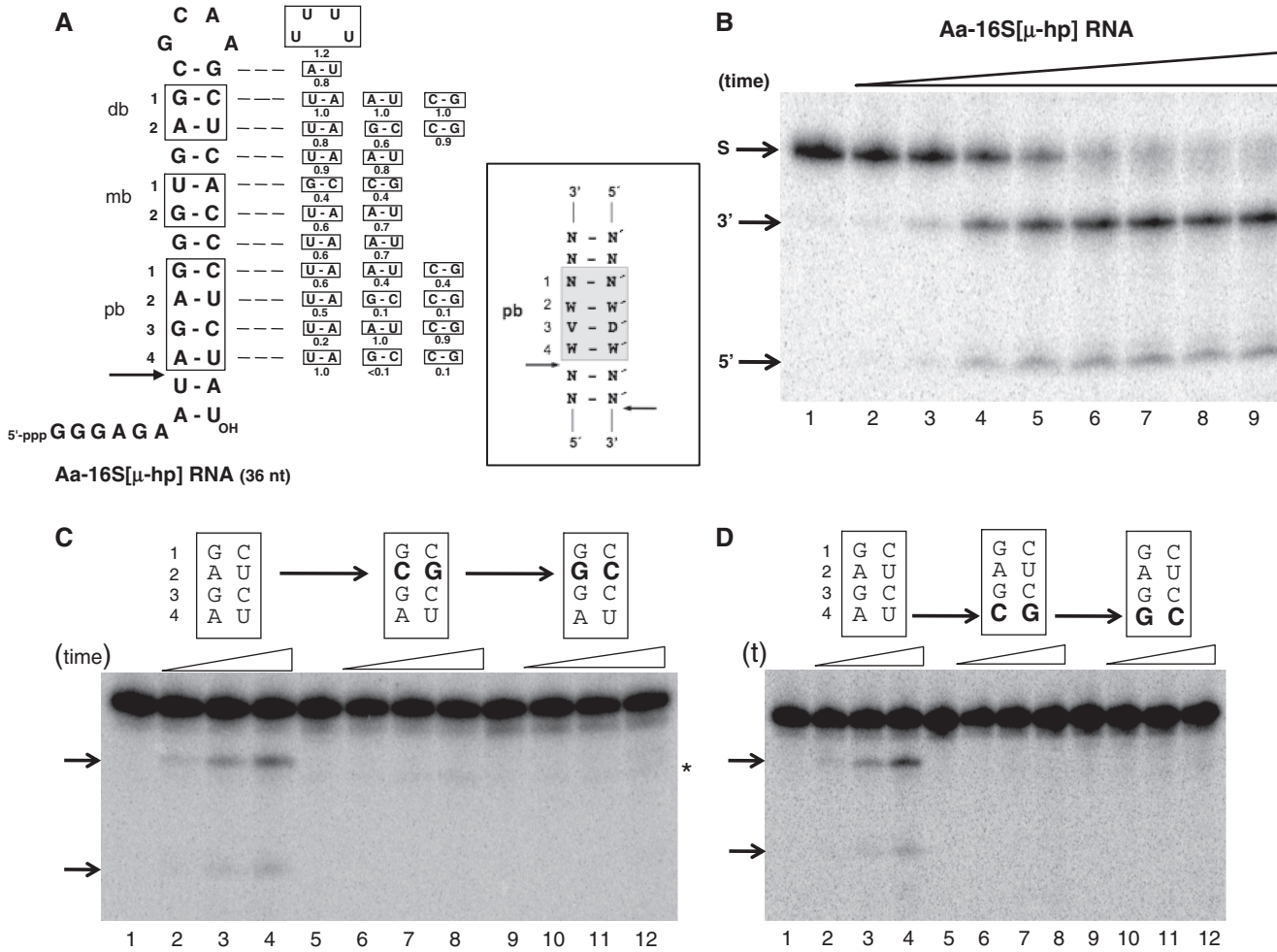

Figure 7. Base-pair sequence dependence of reactivity of a minimal substrate. (**A**) Structure of Aa-16S[μ-hp] RNA. The arrow indicates the Aa-RNase III cleavage site. Also shown are the positions of the distal box (db), middle box (mb) and proximal box (pb), which are sites of protein contact (28,29). The base pair substitutions in the variants and the corresponding relative reactivities are displayed to the right. (**B**) Time course for cleavage of Aa-16S[μ-hp] RNA by Aa-RNase III. The cleavage reaction involved internally ^{32}P-labeled RNA (100 nM) and Aa-RNase III (30 nM) in buffer consisting of 50 mM NaCl, 10 mM $MgCl_2$ and 30 mM Tris–HCl (pH 8). The reaction temperature was 65°C. Lanes 2–9 represent 0.5, 1, 2, 3, 5, 7.5 10 and 20 min time points, respectively. Lane 1 represents incubation of RNA in reaction buffer without enzyme for 20 min. 'S' represents substrate, and 3′ and 5′ represent the cleavage products containing the substrate 3′ and 5′ ends, respectively. (**C**) Cleavage assays of Aa-16S[μ-hp] RNA variants with a CG or GC bp substitution in pb position 2. Reactions involved internally ^{32}P-labeled RNA (500 nM) and Aa-RNase III (10 nM), in 50 mM NaCl, 10 mM $MgCl_2$, 30 mM Tris–HCl (pH 8), incubated at 30°C. Lanes 2–4, 6–8 and 10–12 represent 1, 2 and 5 min reaction times for Aa-16S[μ-hp] RNA and the 2-bp variants (sequences of the respective proximal boxes are shown above the image). Lanes 1, 5 and 9 represent a reaction where RNA was combined with reaction buffer in the absence of enzyme, immediately followed by excess EDTA addition. Arrows indicate the two cleavage products. The asterisk indicates a minor non-enzymatic cleavage product in lanes 5–12. (**D**) Cleavage assays of Aa-16S[μ-hp] RNA variants with a CG or GC bp substitution in pb position 4. Reaction conditions were the same as those in (C). Arrows indicate the two cleavage products. The proximal box sequences of the Aa-16S[μ-hp] RNA variants are shown above the gel images.

secondary structures (42). The extensive base pairing may reflect the ~80°C optimal growth temperature of the *Aquificales* that undoubtedly imposes demanding conditions on rRNA maturation and ribosome assembly (40,41). The placement of the cleavage sites in the pre-16S and pre-23S hairpins is consistent with a role for the enzyme in providing the immediate precursors to the mature rRNAs. Although the *in vivo* RNase III cleavage sites for the Aquifex pre-rRNA substrates are not known, the coincidence of the sites with the *in vitro* sites is anticipated, since in general the *in vitro* processing sites for bacterial RNases III coincide with the *in vivo* sites (1,3,20,39). The activities that provide the mature rRNA 5′- and 3′-ends have not been identified, but may include RNase E/G, which has been implicated in Aquifex 5S rRNA maturation (58,59), and one or more of the 3′→5′ exonucleases identified in Aquifex, including RNase R, RNase PH and polynucleotide phosphorylase (60). The action of RNase III on the primary transcript also would release the precursors to $tRNA^{Ile}$, $tRNA^{Ala}$ and $tRNA^{Arg}$ (Figure 5A). For these species, an RNase P-like activity has been identified in *A. aeolicus* cell-free extracts that can create mature tRNA 5′-ends (61,62), and since the tRNAs already carry the 3′-terminal CCA

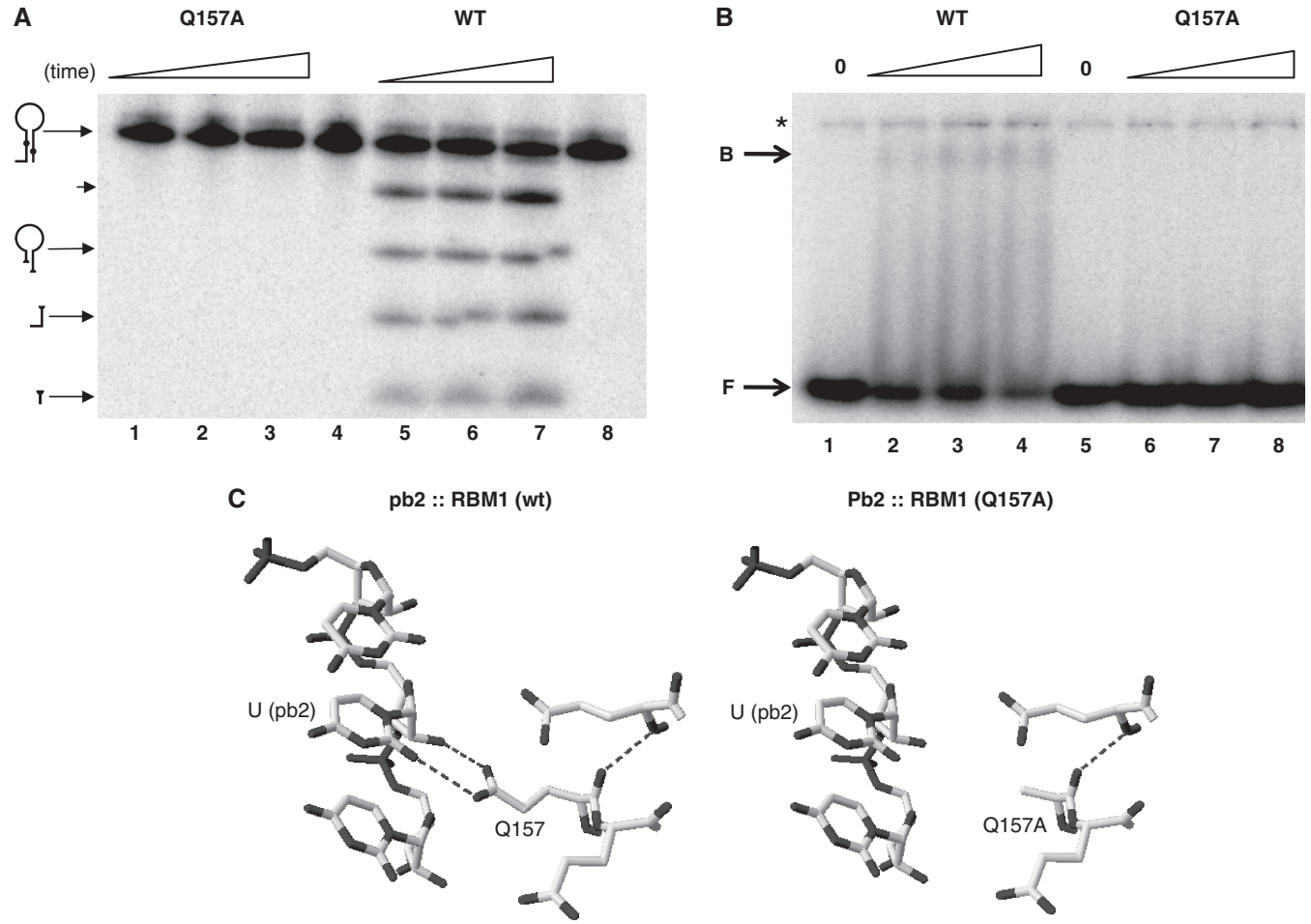

Figure 8. Involvement of the Q157 side chain in substrate binding. (**A**) Cleavage time course assays of Aa-RNase III and the Q157A mutant. Internally ^{32}P-labeled Aa-16S[hp] RNA (400 nM) was combined with Aa-RNase III or the Q157A mutant in 50 mM NaCl, 10 mM $MgCl_2$ and 30 mM Tris–HCl (pH 8). The reaction temperature was 30°C. Lanes 1–3, and 5–7 represent 10, 20 and 40 s reaction times for Q157A and Aa-RNase III (WT), respectively. Lanes 4 and 8 show reactions that lacked Mg^{2+}, but were otherwise complete, and were incubated for 40 s. The figures on the left indicate the positions of the substrate and three cleavage products. The short arrow indicates a product of cleavage of a single phosphodiester at the target site. The slight disruption of two bands in lanes 6 and 7 reflect a physical discontinuity in the gel. (**B**) Gel shift assay of Aa-RNase III (WT) and the Q157A mutant binding to Aa-16S[hp] RNA. Aa-RNase III at the specified concentration (see below) and 5′-^{32}P-labeled Aa-16S[hp] RNA were combined in gel shift buffer, incubated, then electrophoresed in a non-denaturing polyacrylamide gel as described in 'Materials and Methods' section. Reactions were visualized by phosphorimaging. Lanes 1–4 and 5–8 represent reactions containing 0, 100, 200 and 400 nM (dimer concentration) of Aa-RNase III or the Q157A mutant, respectively. The positions of free (F) and bound (B) RNA are indicated. The asterisk indicates the origin of electrophoresis. (**C**) Diagram, based on Figure 4B in reference [28] (PDB: 2EZ6) showing the interaction of the Q157 side chain of Aa-RNase III with uridine at pb position 2. The Q157 side chain and uridine residue are shown, but the paired adenine is not shown. The two hydrogen bonds are indicated by dotted lines, and involve the uracil O2 atom and the ribose 2′-OH group interacting with the Q157 carboxamide group.

sequence, the 3′-ends can be directly fashioned through exonucleolytic trimming by one or more of the 3′→5′ exoribonucleases listed above.

The minimal substrate, Aa-16S[μ-hp] RNA, allowed determination of the K_m and k_{cat} for an Aa-RNase III-catalyzed reaction, as well the characterization of base pair sequence control of substrate reactivity. The reactivity of Aa-16S[μ-hp] RNA is independent of the distal box sequence, which differs from the strong db sequence dependence seen with Ec-RNase III substrates (46,47). The db is a site of contact by one or more residues within a NucD region termed RBM4, which exhibits variability in length and sequence (Figure 1C) (28,29). For Aa-RNase III, the db-RBM4 interaction involves a ribose 2′-OH group that is hydrogen bonded to the R97 side chain (28). Thus, the db sugar-phosphate backbone appears to play a predominant role in recognition, at least by Aa-RNase III. Thus, while the db-RBM4 interaction *per se* is conserved, the variability in db sequence dependence, and in the sequence and length of RBM4 suggest an idiosyncratic interaction. Base pair substitutions in the middle box (mb), which is also a site of RNase III interaction with the sugar-phosphate backbone (28,29), have moderate effects on reactivity. This may reflect local subtle changes in helical structure caused by the base pair substitutions (28,29).

The pb sequence plays a key role in determining Aa-RNase III substrate reactivity. Specific base pair

substitutions within pb positions 2, 3 and 4 reduce reactivity ≥5-fold, and the base pair preference (AU or UA) at positions 2 and 4 is similar to what is observed with Ec-RNase III substrates (47). The uridine at pb position 2 directly interacts with the side chain of Q157 in RBM1 *via* two hydrogen bonds, with one involving the uracil O2 atom, and the other involving the ribose 2′-OH group (Figure 8C) (28,29). Since the UA and AU bp are functionally equivalent, a uridine in either position presumably can engage in energetically equivalent bonding. Inhibition of substrate binding by the Q157A mutation therefore would reflect the loss of two hydrogen bonds, or ∼2–4 kcal/mol of binding energy (63). The functional importance of this interaction is further underscored by the observation that a GC or CG bp substitution at pb position 2 strongly inhibits cleavage. Since Aa-16S[μ-hp] RNA binding to Aa-RNase III could not be detected in a gel shift assay (data not shown), the effect of mutation on enzyme recognition could not be assessed. However, for a minimal substrate of Ec-RNase III, inhibition by a CG or GC bp was attributed to the purine 2-amino group, which is predicted to interfere with positioning of the glutamine side chain (47). A cautionary note is in order, since the crystallographic analyses involved complexes containing cleaved RNAs (28,29). A structural analysis of a pre-catalytic complex would be needed to provide a more precise characterization of the pb–RBM1 interaction. Nonetheless, the data indicate that the RNase III dsRBD engages in sequence specific recognition. Studies are underway to further define the role of dsRBD in substrate binding and cleavage, and to explore the sequence-specific binding capabilities of this conserved fold.

SUPPLEMENTARY DATA

Supplementary Data are available at NAR Online.

ACKNOWLEDGEMENTS

The authors thank Xinhua Ji and Donald Court for helpful discussions over the course of this project, and Robert Huber for providing a sample of *A. aeolicus* DNA. The authors also thank the other members of the laboratory for their advice and encouragement.

FUNDING

Funding for open access charge: National Institutes of Health (GM56772 to A.W.N.).

Conflict of interest statement. None declared.

REFERENCES

1. Court,D.L. (1993) RNA processing and degradation by RNase III. In Belasco,J.G. and Brawerman,G. (eds), *Control of Messenger RNA Stability*. Academic Press, New York, pp. 71–116.
2. LaMontagne,B., Larose,S., Boulanger,J. and AbouElela,S. (2001) The RNase III family: a conserved structure and expanding functions in eukaryotic dsRNA metabolism. *Curr. Issues Mol. Biol.*, **3**, 71–78.
3. Nicholson,A.W. (2003) The ribonuclease III superfamily: forms and functions in RNA maturation, decay, and gene silencing. In Hannon,G.J. (ed.), *RNAi: A Guide to Gene Silencing*. Cold Spring Harbor Laboratory Press, Cold Spring Harbor, NY, pp. 149–174.
4. Drider,D. and Condon,C. (2004) The continuing story of endoribonuclease III. *J. Mol. Microbiol. Biotechnol.*, **8**, 195–200.
5. Carmell,M.A. and Hannon,G.J. (2004) RNase III enzymes and the initiation of gene silencing. *Nat. Struct. Mol. Biol.*, **11**, 214–218.
6. MacRae,I.J. and Doudna,J.A. (2007) Ribonuclease revisited: structural insights into ribonuclease III family enzymes. *Curr. Opin. Struct. Biol.*, **17**, 138–145.
7. Jaskiewicz,L. and Filipowicz,W. (2008) Role of Dicer in posttranscriptional gene silencing. *Curr. Top. Microbiol. Immunol.*, **320**, 77–97.
8. Cuellar,W.J., Kreuze,J.F., Rajamäki,M.-L., Cruzado,K.R., Untiveros,M. and Valkonen,J.P.T. (2009) Elimination of antiviral defense by viral RNase III. *Proc. Natl Acad. Sci. USA*, **106**, 10354–10358.
9. Zhang,Y., Calin-Jageman,I., Gurnon,J.R., Choi,T.J., Adams,B., Nicholson,A.W. and van Etten,J.L. (2003) Characterization of a chlorella virus PBCV-1 encoded ribonuclease III. *Virology*, **317**, 73–83.
10. Carnes,J., Trotter,J.R., Ernst,N.L., Steinberg,A. and Stuart,K. (2005) An essential RNase III insertion editing endonuclease in *Trypanosoma brucei*. *Proc. Natl Acad. Sci. USA*, **102**, 16614–16619.
11. Hernandez,A., Panigrahi,A., Cifuentes-Rojas,C., Sacharidou,A., Stuart,K. and Cruz-Reyes,J. (2008) Determinants for association and guide RNA-directed endonuclease cleavage by purified RNA editing complexes from *Trypanosoma brucei*. *J. Mol. Biol.*, **381**, 35–48.
12. Srivastava,A. and Schlessinger,D. (1990) Mechanism and regulation of bacterial ribosomal RNA processing. *Annu. Rev. Microbiol.*, **44**, 105–129.
13. Deutscher,M.P. (2009) Maturation and degradation of ribosomal RNA in bacteria. *Prog. Mol. Biol. Transl. Sci.*, **85**, 369–391.
14. Price,B., Adamidis,T., Kong,R. and Champness,W. (1999) A *Streptomyces coelicolor* antibiotic regulatory gene, *abs*B, encodes an RNase III homolog. *J. Bacteriol.*, **181**, 6142–6151.
15. Huntzinger,E., Boisset,S., Saveanu,C., Benito,Y., Geissmann,T., Namane,A., Lina,G., Etienne,J., Ehresmann,B., Ehresmann,C. *et al.* (2005) *Staphylococcus aureus* RNAIII and the endoribonuclease III coordinately regulate *spa* gene expression. *EMBO J.*, **24**, 824–835.
16. Saito,H. and Richardson,C.C. (1981) Processing of mRNA by ribonuclease III regulates expression of gene 1.2 of bacteriophage T7. *Cell*, **27**, 533–542.
17. Schmeissner,U., McKenney,K., Rosenberg,M. and Court,D. (1984) Removal of a terminator structure by RNA processing regulates *int* gene expression. *J. Mol. Biol.*, **176**, 39–53.
18. Watkins,K.P., Kroeger,T.F., Cooke,A.M., Williams-Carrier,R.E., Friso,G., Belcher,S.E., van Wijk,K.J. and Barkan,A. (2007) A ribonuclease III domain protein functions in group II intron splicing in maize chloroplasts. *Plant Cell*, **19**, 2606–2623.
19. Dunn,J.J. (1982) Ribonuclease III. In Boyer,P. (ed.), *The Enzymes*, Vol. 15. Academic Press, New York, pp. 485–499.
20. Dunn,J.J. and Studier,F.W. (1983) Complete nucleotide sequence of bacteriophage T7 and the locations of T7 genetic elements. *J. Mol. Biol.*, **166**, 477–535.
21. Calin-Jageman,I. and Nicholson,A.W. (2003) Mutational analysis of an RNA internal loop as a reactivity epitope for *Escherichia coli* ribonuclease III substrates. *Biochemistry*, **42**, 5025–5034.
22. Meng,W. and Nicholson,A.W. (2008) Heterodimer-based analysis of subunit and domain contributions to double-stranded RNA processing by *Escherichia coli* RNase III *in vitro*. *Biochem. J.*, **410**, 39–48.
23. Redko,Y., Bechhofer,D.H. and Condon,C. (2008) Mini-III, an unusual member of the RNase III family of enzymes, catalyzes 23S ribosomal RNA maturation in *B. subtilis*. *Mol. Microbiol.*, **68**, 1096–1106.

24. Redko,Y. and Condon,C. (2009) Ribosomal protein L3 bound to 23S precursor rRNA stimulates its maturation by mini-III ribonuclease. *Mol. Microbiol.*, **71**, 1145–1154.
25. Blaszczyk,J., Tropea,J.E., Bubunenko,M., Routzahn,K.M., Waugh,D.S., Court,D.L. and Ji,X. (2001) Crystallographic and modeling studies of RNase III suggest a mechanism for double-stranded RNA cleavage. *Structure*, **9**, 1225–1236.
26. Blaszczyk,J., Gan,J., Tropea,J.E., Court,D.L., Waugh,D.S. and Ji,X. (2004) Noncatalytic assembly of ribonuclease III with double-stranded RNA. *Structure*, **12**, 457–466.
27. Gan,J., Tropea,J.E., Austin,B.P., Court,D.L., Waugh,D.S. and Ji,X. (2005) Intermediate states of ribonuclease III in complex with double-stranded RNA. *Structure*, **13**, 1435–1442.
28. Gan,J., Tropea,J.E., Austin,B.P., Court,D.L., Waugh,D.S. and Ji,X. (2006) Structural insight into the mechanism of double-stranded RNA processing by ribonuclease III. *Cell*, **124**, 355–366.
29. Gan,J., Shaw,G., Tropea,J.E., Waugh,D.S., Court,D.L. and Ji,X. (2008) A stepwise model for double-stranded RNA processing by ribonuclease III. *Mol. Microbiol.*, **67**, 143–154.
30. Ji,X. (2008) The mechanism of RNase III action: how dicer dices. *Curr. Topics Microbiol. Immunol.*, **320**, 99–116.
31. He,B., Rong,M., Lyakhov,D., Gartenstein,H., Diaz,G., Castagna,R., McAllister,W.T. and Durbin,R.K. (1997) Rapid mutagenesis and purification of phage RNA polymerases. *Protein Expr. Purif.*, **9**, 142–151.
32. Amarasinghe,A.K., Calin-Jageman,I., Harmouch,A., Sun,W. and Nicholson,A.W. (2001) *Escherichia coli* ribonuclease III: affinity purification of hexahistidine-tagged enzyme and assays for substrate binding and cleavage. *Methods Enzymol.*, **342**, 143–158.
33. Meng,W., Nicholson,R.H., Nathania,L., Pertzev,A.V. and Nicholson,A.W. (2008) New approaches to understanding double-stranded RNA processing by ribonuclease III. Purification and assays of homodimeric and heterodimeric forms of RNase III from bacterial extremophiles and mesophiles. *Methods Enzymol.*, **447**, 119–129.
34. Milligan,J.F. and Uhlenbeck,O.C. (1989) Synthesis of small RNAs using T7 RNA polymerase. *Methods Enzymol.*, **180**, 51–62.
35. Peattie,D.A. (1979) Direct chemical method for sequencing RNA. *Proc. Natl Acad. Sci. USA*, **76**, 1760–1764.
36. Carey,J., Cameron,V., deHaseth,P.L. and Uhlenbeck,O.C. (1983) Sequence-specific interaction of R17 coat protein with its ribonucleic acid binding site. *Biochemistry*, **22**, 2601–2610.
37. Carey,J. (1991) Gel retardation. *Methods Enzymol.*, **208**, 103–117.
38. Sun,W., Pertzev,A. and Nicholson,A.W. (2005) Catalytic mechanism of *Escherichia coli* ribonuclease III. Kinetic and inhibitor evidence for the involvement of two Mg^{2+} ions in phosphodiester hydrolysis. *Nucleic Acids Res.*, **33**, 807–815.
39. Dunn,J.J. (1976) RNase III cleavage of single-stranded RNA. Effect of ionic strength on the fidelity of cleavage. *J. Biol. Chem.*, **251**, 3807–3814.
40. Deckert,G., Warren,P.V., Gaasterland,T., Young,W.G., Lenox,A.L., Graham,D.E., Overbeek,R., Snead,M.A., Keller,M., Aukjay,M. *et al.* (1998) The complete genome of the hyperthermophilic bacterium *Aquifex aeolicus*. *Nature*, **392**, 353–358.
41. Swanson,R.V. (2001) Genome of *Aquifex aeolicus*. *Methods Enzymol.*, **330**, 158–169.
42. Saito,R., Ozawa,Y., Kuzuno,N. and Tomita,M. (2000) Computer analysis of potential stem structures of rRNA operons in various procaryotic genomes. *Gene*, **259**, 217–222.
43. Young,R.A. and Steitz,J.A. (1978) Complementary sequences 1700 nucleotides apart form a ribonuclease III cleavage site in *Escherichia coli* ribosomal precursor RNA. *Proc. Natl Acad. Sci. USA*, **75**, 3593–3597.
44. Bram,R.J., Young,R.A. and Steitz,J.A. (1980) The ribonuclease III site flanking the 23S sequence in the 30S ribosomal precursor RNA of *E. coli*. *Cell*, **19**, 393–401.
45. Li,H. and Nicholson,A.W. (1996) Defining the enzyme binding domain of a ribonuclease III processing signal. Ethylation interference and hydroxyl radical footprinting using catalytically inactive RNase III mutants. *EMBO J.*, **15**, 1421–1433.
46. Zhang,K. and Nicholson,A.W. (1997) Regulation of ribonuclease III processing by double-helical sequence antideterminants. *Proc. Natl Acad. Sci. USA*, **94**, 13437–13441.
47. Pertzev,A. and Nicholson,A.W. (2006) Characterization of RNA sequence determinants and antideterminants of processing reactivity for a minimal substrate of *Escherichia coli* ribonuclease III. *Nucleic Acids Res.*, **34**, 3708–3721.
48. Robertson,H.D., Webster,R.E. and Zinder,N.D. (1968) Purification and properties of ribonuclease III from *Escherichia coli*. *J. Biol. Chem.*, **243**, 82–91.
49. Sun,W. and Nicholson,A.W. (2001) Mechanism of action of Escherichia coli ribonuclease III. Stringent chemical requirement for the glutamic acid 117 side chain, and Mn^{2+} rescue of the Glu117Asp mutant. *Biochemistry*, **40**, 5102–5110.
50. Akey,D.L. and Berger,J.M. (2005) Structure of the nuclease domain of ribonuclease III from *M. tuberculosis* at 2.1 Å. *Protein Sci.*, **14**, 2744–2750.
51. Campbell,F.E., Cassano,A.G., Anderson,V.E. and Harris,M.E. (2002) Pre-steady-state and stopped-flow fluorescence analysis of *Escherichia coli* ribonuclease III: insights into mechanism and conformational changes associated with binding and catalysis. *J. Mol. Biol.*, **317**, 21–40.
52. Cambillau,C. and Claverie,J.-M. (2000) Structural and genomic correlates of hyperthermostability. *J. Biol. Chem.*, **275**, 32383–32386.
53. Suhre,K. and Claverie,J.-M. (2003) Genomic correlates of hyperthermostability, an update. *J. Biol. Chem.*, **278**, 17198–17202.
54. Nathania,L. and Nicholson,A.W. (2010) *Thermotoga maritima* ribonuclease III. Characterization of thermostable biochemical behavior and analysis of conserved base pairs that function as reactivity epitopes for the Thermotoga 23S rRNA precursor. *Biochemistry*, **49**, 7164–7178.
55. Plaxco,K.W., Simons,K.T. and Baker,D. (1998) Contact order, transition state placement and the refolding rates of single domain proteins. *J. Mol. Biol.*, **277**, 985–994.
56. Robinson-Rechavei,M. and Godzik,A. (2005) Structural genomics of *Thermotoga maritima* proteins shows that contact order is a major determinant of protein thermostability. *Structure*, **13**, 857–860.
57. Robinson-Rechavi,M., Alibés,A. and Godzik,A. (2006) Contribution of electrostatic interactions, compactness and quaternary structure to protein thermostability: lessons learned from structural genomics of *Thermotoga maritima*. *J. Mol. Biol.*, **356**, 547–557.
58. Lombo,T.B. and Kaberdin,V.R. (2008) RNA processing in *Aquifex aeolicus* involves RNase E/G and an RNase P-like activity. *Biochem. Biophys. Res. Comm.*, **366**, 457–463.
59. Kaberdin,V.R. and Bizebard,T. (2005) Characterization of *Aquifex aeolicus* RNase E/G. *Biochem. Biophys. Res. Comm.*, **327**, 382–392.
60. Condon,C. and Putzer,H. (2002) The phylogenetic distribution of bacterial ribonucleases. *Nucleic Acids Res.*, **30**, 5339–5346.
61. Wilkomm,D.K., Feltens,R. and Hartmann,R.K. (2002) tRNA maturation in *Aquifex aeolicus*. *Biochimie*, **84**, 713–722.
62. Marszalkowski,M., Willkomm,D.K. and Hartmann,R.K. (2008) 5′-end maturation of tRNA in *Aquifex aeolicus*. *Biol. Chem.*, **389**, 395–403.
63. Lesser,D.R., Kurpiewski,M.R. and Jen-Jacobson,L. (1990) The energetic basis of specificity in the Eco RI endonuclease-DNA interaction. *Science*, **250**, 776–786.